Egypt. J. Chem. **Vol. 67**, No. 7 pp. 201 - 219 (2024)

Egyptian Journal of Chemistry

http://ejchem.journals.ekb.eg/

A Comprehensive Investigation of Corrosion Efficiency of Cu-10Ni Alloy in Hybrid Cr^{3+}/ Ni^{2+} with Tungstate in Chloride Media

Ghalia A. Gaber[a], AliaaAbdelfatah[b], Lamiaa Z. Mohamed[b,*]

[a]*Department of Chemistry, Faculty of Science (Girls), Al-Azhar University, P.O. Box: 11754, Yousef Abbas Str., Nasr City, Cairo, Egypt*

[b]*Mining, Petroleum, and Metallurgical Engineering Department, Faculty of Engineering, Cairo University, 12613, Egypt*

Abstract

Pipes that carry saltwater, and desalination facilities are all typical applications for the Cu-10Ni alloy. Examining the surface characterization and the corrosion performance of Cu-10Ni alloy after immersion in hybrid Cr^{3+}/ Ni^{2+} solutions with tungstate in either 0.5 M HCl or 1 M NaCl. The influence of the addition of hybrid Cr^{3+}/ Ni^{2+} with tungstate on the corrosion of Cu-10Ni alloy in 1M HCl or 0.5M NaCl was investigated with weight loss (WTL) method and open circuit potential (OCP) measurements over 7 days to 90 days. Also, potentiodynamic polarization (POT) and cyclic voltammetry (CYV) were performed. The findings show that tungstate has a low IE in comparison to a hybrid solution containing Cr^{3+}/ or Ni^{2+} ions. The solution's Cl^- continuously assaults the protective layer as immersion time increases, rupturing it. Following 7 days, the tungstate hybrid Cr^{3+} has the highest IE 82%; and 68% in HCl and NaCl, respectively. Thus, the IE values in HCl and NaCl after 90 days were 67.1% and 97.9%, respectively. Furthermore, the hybrid Cr^{3+}/ or Ni^{2+} with tungstate results in a slight difference in the anodic, cathodic, and corrosion potential Tafel constant values. An increase in the IE% values of the hybrid Cr^{3+} with tungstate in HCl and NaCl from 58.0 % to 82.3 % indicates a better surface coverage of the Cu-10Ni alloy. The examination of the surface morphology is accomplished using an energy-dispersive X-ray analysis (EDX) and a scanning electron microscope (SEM).

Keywords: Cu-10Ni alloy; Corrosion behaviour; Inhibitors; Chloride media; Microstructure

1. Introduction

The breakdown or deterioration of metallic materials caused by the contact of the metal surface with the environment is known as the corrosion process [1, 2]. Because metals and other elements gravitate towards their lowest energy states, corrosion is a naturally occurring phenomenon [1]. The corrosion products can generate very thin, defensive, tightly adherent films or pitting films that are very thin and reduce the pace of corrosion [3]. Copper has several applications due to its exceptional characteristics. It is used in hardware to produce wires, and cylinders and also to create alloys [4]. Cu-Ni alloys are used in several applications such as power generation, including automotive, marine, and jet engine compressors industries [5. 6. 7]. Significant interest has been devoted to the investigation of the corrosion characteristics of Cu-Ni alloys because of their exceptional corrosion resistance (CRST) and the intrinsic resistance of Cu alloys to biological pollutants. Diverse Cu-Ni alloys have been reported to corrode in chloride solutions and natural seawater under a range of conditions [8]. Divergent findings have been accumulated; some writers have posited that selective electro-dissolution of Ni predominates, whilst others have discovered that the dissolution of Cu is contingent upon the composition of the alloy [9]. The better CRST of Cu-An elemental cause for the corrosion product coating that develops on the surfaces of Ni alloys may be identified. This coating slows the rate of ion diffusion significantly, resulting in a decrease in the corrosion rate (CR) [10]. The Cu-Ni alloy corrosion product film formed in stagnant

*Corresponding author e-mail: lamiaa.zaky@cu.edu.eg; (Lamiaa Z. Mohamed).
EJCHEM use only: Received date 13 November 2023; revised date 06 December 2023; accepted date 17 December 2023
DOI: 10.21608/EJCHEM.2023.248320.8865
©2024 National Information and Documentation Center (NIDOC)

seawater primarily comprises a porous (Cu, $M)_2(OH)_3Cl$ (where M is Ni, Fe, or Mn) outer layer and a faulty and compact Cu_2O inner layer [11]. The effect of Ni^{2+} on the corrosion characteristics of steel pipelines was also investigated [12]. When submerged in NaCl, the Cu-Ni alloy of the Cu_2O and CuO films with Ni incorporation lowered the cation vacancy concentration, resulting in increased CRST [13]. The enhancement of Cu's CRST by Ni insertion into the corrosion product layer was observed, and an endeavor was undertaken to establish a correlation between the Cu–10Ni alloy's microstructure and corrosion behaviour [14, 15]. Probably because of the selective corrosion of Ni, the inner layer is enriched with Cu and O and deficient in Ni (denickelification) [14]. Cu in the matrix is preferentially dissolved and redeposited to produce Cu_2O film, which possesses semiconductor characteristics because Cl^- is present in the solution. Because nickel is doped into the cationic vacancy of the Cu_2O film in the form of ions after dissolution, which lowers the cationic vacancy concentration and increases the corrosion resistance by reducing the electrical conductivity of the film, the corrosion resistance of Cu–Ni alloy is superior to that of pure Cu [6, 16]. A corrosion inhibitor is defined as a chemical compound that, when introduced into a medium in minute quantities, hinders the degradation of metal caused by the environment in which it is present [17]. Based on their chemical composition, inhibitors may be classified as organic inhibitors, mixed-substance inhibitors, or inorganic inhibitors [18, 19, 20]. Inhibitors might be incorporated into the varnish or applied directly to the surface to enhance the corrosion resistance [21, 22]. The protective action of WO_4^{2-} in distilled water is approximately identical in the presence of corrosive ions. WO_4^{2-} was found to be more effective, and the toxicity is very low. Furthermore, the use of tungstate in isolation as a corrosion inhibitor in industrial cooling water systems is not feasible due to its substantial cost and restricted oxidizing capability. Extensive research has been conducted on the application of co-inhibitors [23, 24, 25]. Cr is a transition metal element that is frequently employed as an alloying element to raise the CRST of alloys which is comparable with Ni in atomic radii and electron configurations. It has examined the electrochemical characteristics of Cu-Ni alloys with various alloying elements and shown that Cr can lower the alloy's CR and corrosion current density. It did not, however, provide a detailed explanation of the mechanism of Cr on the CRST of Cu-Ni alloys or indicate the evolution of Cr in the corrosion product layer. There aren't many studies on the impact of Cr on Cu-Ni alloy corrosion behaviour and mechanism that have been published to date. Consequently, it is worthwhile to investigate how micro-alloying Cr elements can raise Cu-Ni alloys' CRST [13].

Since the Cu-10Ni alloy's corrosion mechanism is more complicated, there has been a lot of research on its mechanical characteristics and corrosion resistance; however, the research to date is not sufficiently comprehensive [6]. This study examined the enhancement of corrosion characteristics of Cu-10Ni alloy in hybrid Cr^{3+} or Ni^{2+} with tungstate in 1M HCl and 0.5M NaCl medias employing weight loss (WTL), open circuit potential (OCP), potentiodynamic polarization (POT), and cyclic voltammetry (CYV) for 7 and 90 days. The corrosion products on the alloy with different inhibitions were characterized by their morphology by scanning electron microscopy (SEM), their elemental composition by energy dispersive X-ray analysis (EDX), and their elemental distribution by mapping.

2.Experimental Work

2.1 Preparation of the Specimens The working electrode with dimensions 20x20x2 mm^3 was fabricated from a Cu-10Ni alloy sheet with the following chemical composition (wt. %): 9.27% Ni; 0.768% Mn; 1.67% Fe, and 88.24% Cu. The electrode was polished to a mirror finish, decreased with acetone, and utilized for the WTL, POT, and surface inspection investigations.

2.2 Weight Loss (WTL) Seven days were spent immersing Cu-10Ni alloy in 50 ml of 1 M HCl or 0.5 M NaCl with 0.1 M inhibitor concentrations with/without hybrid Cr^{3+}/ or Ni^{2+} with tungstate. The average CR may then be calculated using Eqs.1 and 2. [26. 27, 28]:

$$\Delta W = W_1 - W_2 \quad (1)$$

$$C.R.(mm/y) = \frac{\Delta W \times K}{A \times T \times D} \quad (2)$$

Where K represents a constant ($8.76x10^4$), T provides the exposure time in days. A gives the area in cm^2, ΔW indicates WTL in grams, and D represents the density of the Cu-10Ni alloy (8.9 g/cm^3). The surface coverage degree (θ) was calculated using Eq. 3:

$$\theta = \frac{W_0 - W_i}{W_0} \quad (3)$$

Where Wi and W_0 are the values of WTL of Cu-10Ni alloy with/without inhibition, respectively. The inhibition efficiency percentage ($IE\%$) was calculated according to Eq. 4:

$$IE\% = \theta \times 100 \quad (4)$$

2.3. Open circuit potential (OCP)
The 1 M HCl or 0.5 M NaCl electrochemical behaviour containing varied inhibitor concentrations in the presence and absence of hybrid Cr^{3+}/ or Ni^{2+} with tungstate was examined by measuring the change in corrosion potential (E_{corr}) over 7 days. The steady-state OCP was subjected to electrochemical measurements. During a 30 min exposure period, the OCP time dependency for several tests was recorded.

2.4. Potentiodynamic polarization (POT)
The scanning rate of 5 mVs^{-1} was used to alter the electrode potential from -0.7 to +0.7 V to capture POT curves. A laptop and a VoltaMaster PGZ 301 potentiostat/galvanostat linked to a three-electrode cell assembly were used to conduct measurements of corrosion inhibition. Saturated calomel electrode (SCE), Cu-10Ni alloy, and platinum wire serve as the reference electrode, the working electrode, and the counter electrode in this cell, respectively. To calculate current densities (I_{corr}), Tafel polarization analysis of anodic and cathodic curves was performed. Using Eq. 5, the inhibitive efficiency (IE%) was computed.

$$IE = \left(1 - \frac{CR_{inh}}{CR_0}\right) x\ 100 \qquad (5)$$

where CR_0 and CR_{inh} are the CR values in the absence and presence of hybrid Cr^{3+}/ or Ni^{2+} with tungstate, respectively.

2.5 Cyclic voltammetry (CYV) The CYV offers a qualitative insight into pitting corrosion mechanisms. It is also a highly useful method for determining a metal or alloy's susceptibility to pitting in a specific corrosive environment. Cu-10Ni alloy was subjected to CYV experiments in chloride media (1 M HCl and 0.5 M NaCl) in both the absence/presence of hybrid Cr^{3+}/ or $Ni^{2+}$with tungstate using a potentiostat model PGZ301. The potential was first measured at a cathodic direction and then allowed to sweep to an anodic direction until a sharp change in the current's direction in the active direction was seen. After that, a second cathodic sweep of the sample was performed.

2.6 Surface Examination The Cu-10Ni alloy was submerged in different test solutions for 7 and 90 days. After two intervals, the specimens were extracted and dried. Surface analysis used the SEM, and EDX analysis to ascertain the characteristics of the coating that forms on the metal sample's surfaces.

3. Results and Discussions
3.1 Influence of immersion period
The WTL approach quantified the increase in CRST of Cu-10Ni alloys containing hybrid Cr^{3+}/ or Ni^{2+} when coated with tungstate. Figs. 1 and 2 depict the WTL-Time curves for corrosion of Cu-10Ni alloy in hybrid Cr^{3+}/ or Ni^{2+} with tungstate in chloride medium after 7 days and 90 days, respectively. Tables 1 and 2 display the C.R. and Inhibition Efficiency (IE%) of Cu-10Ni alloy in chloride medium (1 M HCl and 0.5 M NaCl) in hybrid Cr^{3+}/ or Ni^{2+} with tungstate after 7 days and 90 days, respectively. The immersion time of 7 days was performed to indicate the early-stage corrosion behaviour of the Cu-10Ni alloy. The tungstate hybrid Cr^{3+} has the greatest IE percent after 7 days, 82%: 68% in HCl and NaCl, respectively. According to the results, tungstate alone has a low IE, when compared to a hybrid Ni^{2+} ion solution or a hybrid with Cr^{3+} ions. Corrosion accelerates in the absence of hybrid Cr^{3+}/ or Ni^{2+} with tungstate or tungstate alone. When tungstate is coupled with Cr^{3+}/ or Ni^{2+}ions, the IE increases in both HCl and NaCl, which are corrosive environments. As immersion time grows, the effectiveness of the inhibition reduces [29]. As immersion time rises, the Cl^- in the solution continuously attacks the protective layer, causing it to rupture. Thus, the greatest IE percentages in HCl and NaCl after 90 days, were 67.1 and 97.9, respectively.

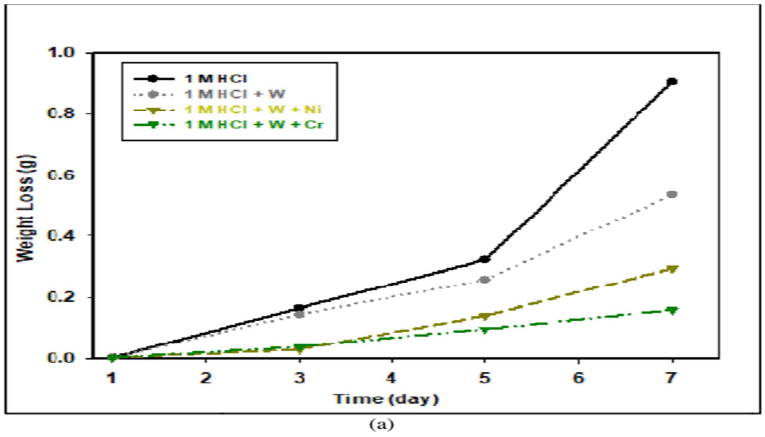

(a)

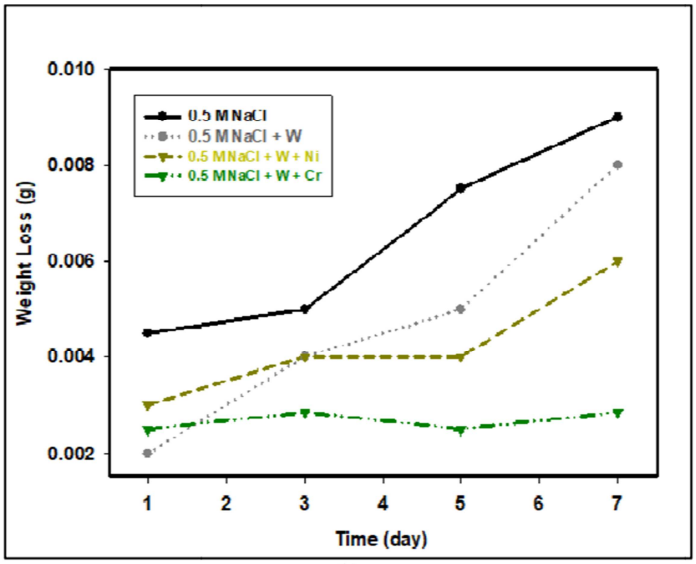

(b)

Figure 1: WTL-Time plots for the Cu-10Ni alloy corroded in hybrid Cr^{3+}/ or Ni^{2+} with tungstate after 7 days in (a) 1 M HCl and (b) 0.5 M NaCl

Table 1. The CR and the Inhibition efficiency (I.E. %) of Cu-10Ni alloy in hybrid Cr^{3+}/ or Ni^{2+} with tungstate in chloride mediaby WTL method after 7 days

Inhibitors	1M HCl			0.5 M NaCl		
	WTL, (g)	CR., mm/y	IE %	WTL, (g)	CR., mm/y	IE %
Cu-Ni alloy	0.905	318.06	--	0.009	3.16	--
Cu-Ni alloy +(W)	0.536	188.42	41.2	0.008	2.81	11.2
Cu-Ni alloy +(W+Ni)	0.295	103.52	67.1	0.006	2.11	33.1
Cu-Ni alloy +(W+Cr)	0.159	55.89	82.2	0.003	1.00	68.1

Table 2. The CR and the Inhibition efficiency (I.E. %) of Cu-10Ni alloy in hybrid Cr^{3+}/ or Ni^{2+} with tungstate in chloride mediaby WTL method after 90 days

Inhibitors	1M HCl			0.5 M NaCl		
	WTL, (g)	CR., mm/y	IE %	WTL, (g)	CR., mm/y	IE %
Cu-Ni alloy	1.099	30.05	--	0.1585	4.334	--
Cu-Ni alloy +(W)	0.799	21.83	27.3	0.0220	0.602	86.1
Cu-Ni alloy +(W+Ni)	0.601	16.42	45.4	0.0085	0.232	94.6
Cu-Ni alloy +(W+Cr)	0.362	9.88	67.1	0.0032	0.088	97.9

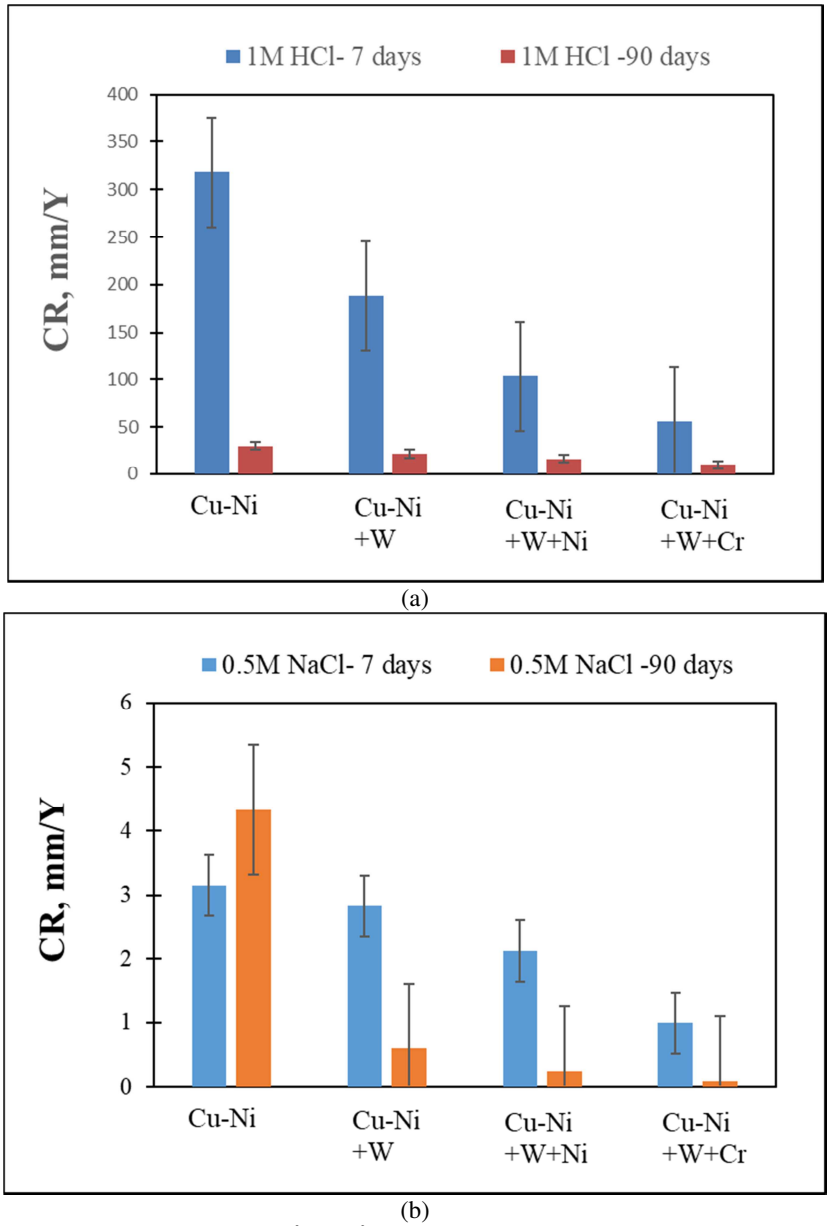

Figure 2: The CR values of Cu-10Ni alloy in hybrid Cr^{3+}/ or Ni^{2+} with tungstate after 7 and 90 days in (a) 1M HCl, and (b) 0.5 M NaCl

3.2 Open circuit potential

Figure 3 depicts the E_{corr}, fluctuation with time for the Cu-10Ni alloy corroded in hybrid Cr^{3+}/ or Ni^{2+} with tungstate in chloride medium after 7 days. The E_{corr} exhibits a positive displacement of around 50 mV and a corrosion time of 7 days. This is attributed to the protective oxide coating, which acts as an inhibitory effect and causes corrosion on the Cu-10Ni surface by reducing the reaction rate [30]. A reduction in Cl^-attack on the alloy surface and the formation of a protective oxide coating resulted in a decline in CR and homogeneous corrosion of Cu-10Ni alloy. Frequently, first-stage corrosion results in a smooth Cu-10Ni matrix. Activation regulates the surface corrosion of the matrix due to the free diffusion of Cl^- ions, dissolved oxygen, and corrosion products. Through Cl^- interaction, marine Cu is oxidized to CuO in the passivation zone, Cu_2O in the activation zone, and chloride. Cu_2O, which is thermally unstable, oxidizes readily to Cu ions. The Cu_2O layer thickens, and a corrosion product coating develops on the matrix during immersion. Halogen ion, dissolved oxygen, and corrosion product diffusion are all reduced with the combination of protective oxide and corrosion product coatings. Due to the increased potential, Cl adsorbed on the surface layer, thickening the Cu_2O film, which resulted in the

formation of cupric chloride hydroxide ($Cu_2(OH)_3Cl$), a porous, green corrosion product [31]. Continuous Cl^- penetrates CuO film flaws and decreases protective film resistance, causing localized collapse as corrosion continues. The vigorous assault of Cl^- causes substrate pitting and microvoid development [32]. The Cu dissolution creates new corrosion active sites, which inhibits protective coating and worsens localized surface corrosion.

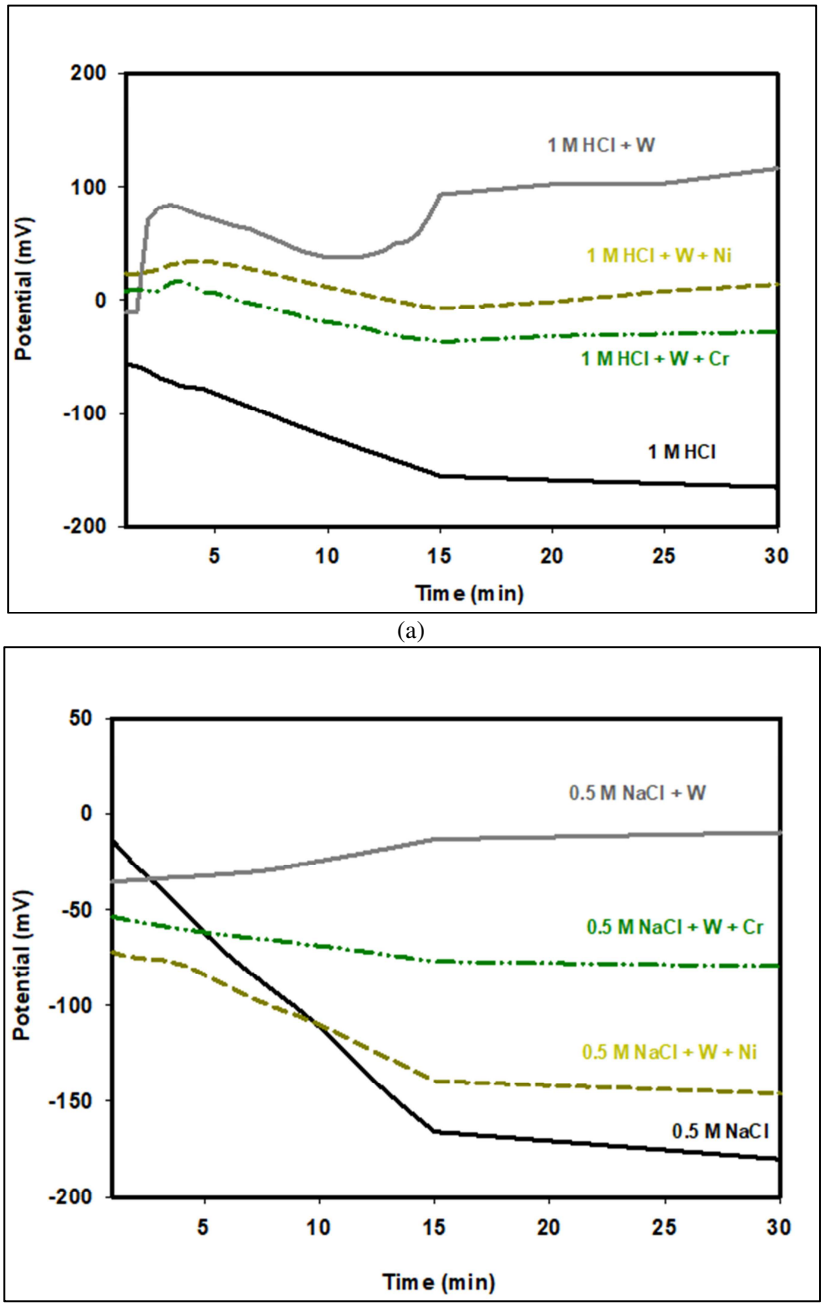

Figure 3: The potential vs. time for the Cu-10Ni alloy corroded in hybrid Cr^{3+}/ or Ni^{2+} with tungstate after 7 days in (a) 1M HCl, and (b) 0.5 M NaCl

3 POT measurements

The POT curvesfor Cu-10Ni alloy in hybrid Cr^{3+}/ or Ni^{2+} with tungstate in 1 M HCl or 0.5 M NaCl after immersion 90 days are shown in Fig. 4. The curves in the image trend toward less current and less negative

potential, as seen by carefully examining it. This finding points to the additive hybrid Cr^{3+}/ or Ni^{2+} with a tungstate inhibitory effect. The values of potential corrosion (E_{corr}), Tafel slopes (β_a, β_c), current density (I_{corr}), and rates of corrosion (CR) of Cu-10Ni alloy in hybrid Cr^{3+}/ or Ni^{2+} with tungstate in 1M HCl or 0.5 M NaClare presented in Tables 3, and 4, respectively. The results demonstrate that adding Cr with tungstate for Cu-Ni alloysreduces I_{corr} values, which decreases the reduction with adding Ni to Cr. The alloy's interaction with the Cu through adsorption, which obstructs more active corrosion sites, may be responsible for the decrease in CR. This outcome is in line with the data from measurements of weight reduction. Additionally, the presence of hybrid Cr^{3+}/ or Ni^{2+} with tungstate causes a little variation in the values of the Tafel constants for the anodic, cathodic, and corrosion potential. According to these findings, the additive functions as a mixed-type inhibitor. This indicates that the molecules of the additive adhere to the anodic and cathodic surfaces of the alloy. A higher surface coverage of the Cu-10Ni alloy is indicated by an increase in the (IE%) values of the hybrid Cr^{3+} with tungstate in HCl and NaCl from 58.0 % to 82.3 %.

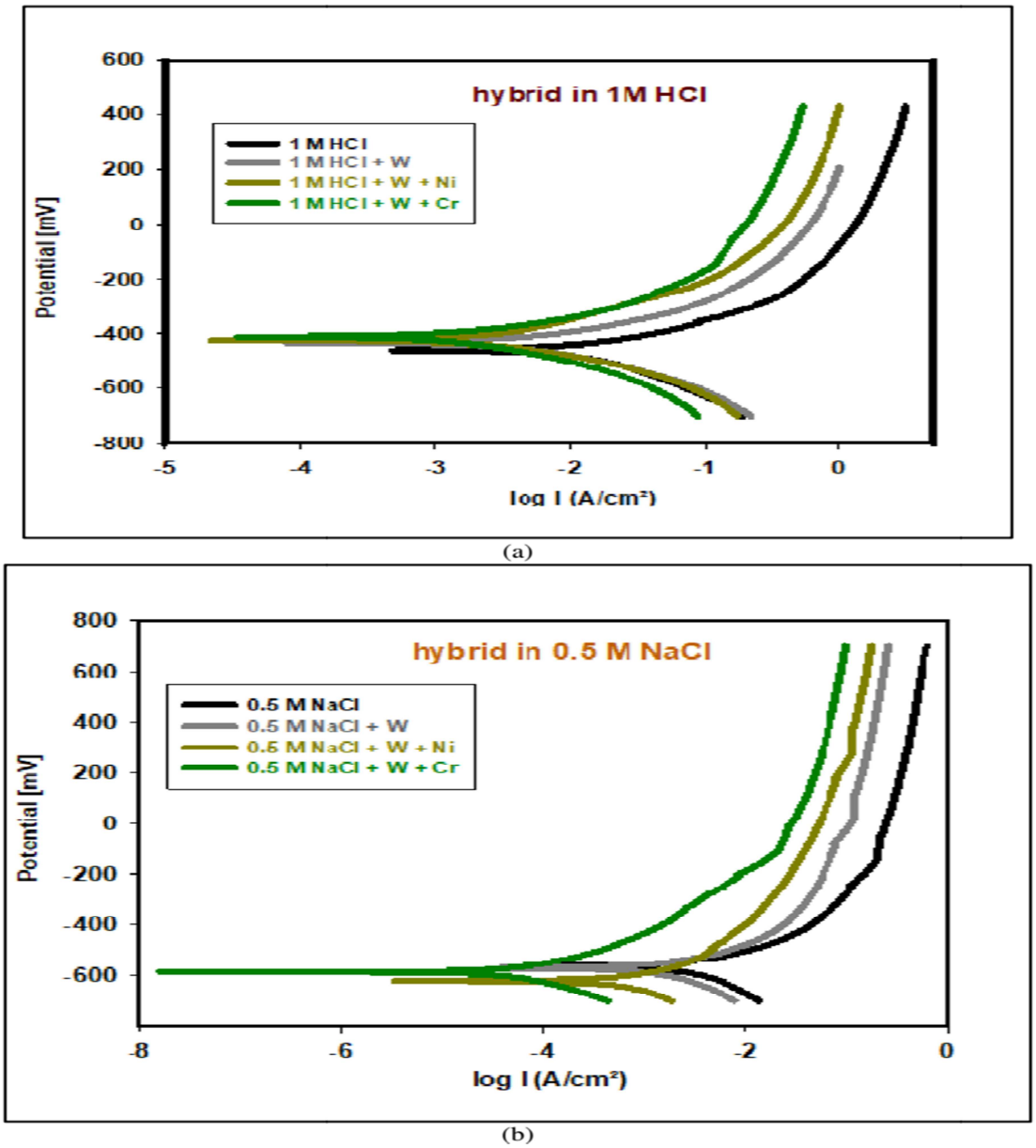

Figure 4: POT plots for Cu-10Ni alloy in hybrid Cr^{3+}/ or Ni^{2+} with tungstate after immersion 90 days in (a) 1 M HCl and (b) 0.5 M NaCl

Table 3. POT parametersof Cu-10Ni alloy in hybrid Cr^{3+}/ or Ni^{2+} with tungstate in 1M HCl

Inhibitors	E_{corr} mV	I_{corr} mA/cm^2	β_a mV/dec	β_c mV/dec	*CR* mm/y	θ	*IE %*
Cu-Ni alloy	-465.5	4.0789	104.5	-171.8	47.70	--	--
Cu-Ni alloy +(W)	-438.6	3.6517	90.7	-109.0	42.71	0.105	10.5
Cu-Ni alloy +(W+Ni)	-429.8	2.8311	135.7	-99.0	33.11	0.306	30.6
Cu-Ni alloy +(W+Cr)	-417.9	1.7127	91.4	-116.9	20.03	0.580	58.0

Table 4. POT of parametersof Cu-10Ni alloy in hybrid Cr^{3+}/ or Ni^{2+} with tungstate in 0.5 M NaCl

Inhibitors	E_{corr} mV	I_{corr} mA/cm^2	β_a mV/dec	β_c mV/dec	*CR* mm/y	θ	*IE %*
Cu-Ni alloy	-569.8	1.7036	106.7	-194.4	19.92	--	--
Cu-Ni alloy +(W)	-577.1	1.4654	104.4	-172.5	17.14	0.139	13.9
Cu-Ni alloy +(W+Ni)	-628.4	0.5702	105.3	-150.1	6.668	0.665	66.5
Cu-Ni alloy +(W+Cr)	-592.3	0.3021	99.8	-124.3	3.533	0.823	82.3

3.4 Cyclic voltammetry (CYV)

Fig. 5 depicts the CYV curves for Cu-10Ni alloy in hybrid Cr^{3+}/ or Ni^{2+} with tungstate in 1 M HCl or 0.5 M NaCl after immersion for 90 days. The CYV corrosion parameters such as E_{corr}, E_{pitt}, E_{prot}, *CR,*and I_{corr}, are listed in Tables 5 and 6. The hybrid Cr^{3+}/ $Ni^{2+}$with tungstate exhibits consistent passive characteristics throughout a broad potential range, followed by an increase in E_{corr} values towards more negative values in comparison to the addition of 1 M HCl or 0.5 M NaCl to Cu-10Ni alloy free. The sample exhibited enhanced efficiency after the introduction of hybrid Cr^{3+}/ Ni^{2+}, as shown by the complete elimination of the hysteresis loop seen during the inverse anodic scan, which served as an indicator of pitting corrosion. Commonly, the CYV curves' hysteresis loop area immediately indicates localized corrosion. For instance, a large hysteresis loop area implies corrosion vulnerability. The reverse anodic scan shows a hysteresis loop, suggesting pitting. The passive surface pitting is caused by chloride ions competing for adsorption at the metal/oxide layer contact. At a certain chloride concentration, a pitting potential displaces oxygen from the protective oxide layer.

Table 5 The CYV plots parameters forCu-10Ni alloy in hybrid Cr^{3+}/ or Ni^{2+} with tungstate in 1M HCl

Inhibitors	E_{corr} (V/SCE)	I_{corr} (mA/cm²)	E_{pit}(V/SCE)	E_{prot} (V/SCE)	θ	IE (%)
Cu-Ni alloy	-0.4615	19.3010	0.1905	-0.4485	--	--
Cu-Ni alloy +(W)	-0.4674	11.9578	0.1695	-0.4140	0.381	38.1
Cu-Ni alloy +(W+Ni)	-0.4745	10.4637	0.1650	-0.4562	0.458	45.8
Cu-Ni alloy +(W+Cr)	-0.4732	7.2562	0.1471	-0.4484	0.624	62.4

Table 6 The CYV plots parameters forCu-10Ni alloy in hybrid Cr^{3+}/ or Ni^{2+} with tungstate in 0.5 M NaCl

Inhibitors	E_{corr} (V/SCE)	I_{corr} (mA/cm²)	E_{pit}(V/SCE)	E_{prot} (V/SCE)	θ	IE (%)
Cu-Ni alloy	-0.5771	1.4654	0.1878	-0.5581	--	--
Cu-Ni alloy +(W)	-0.5703	0.7884	0.1815	-0.5492	0.462	46.2
Cu-Ni alloy +(W+Ni)	-0.5712	0.7278	0.1800	-0.5610	0.503	50.3
Cu-Ni alloy +(W+Cr)	-0.5777	0.5799	0.1755	-0.5473	0.604	60.4

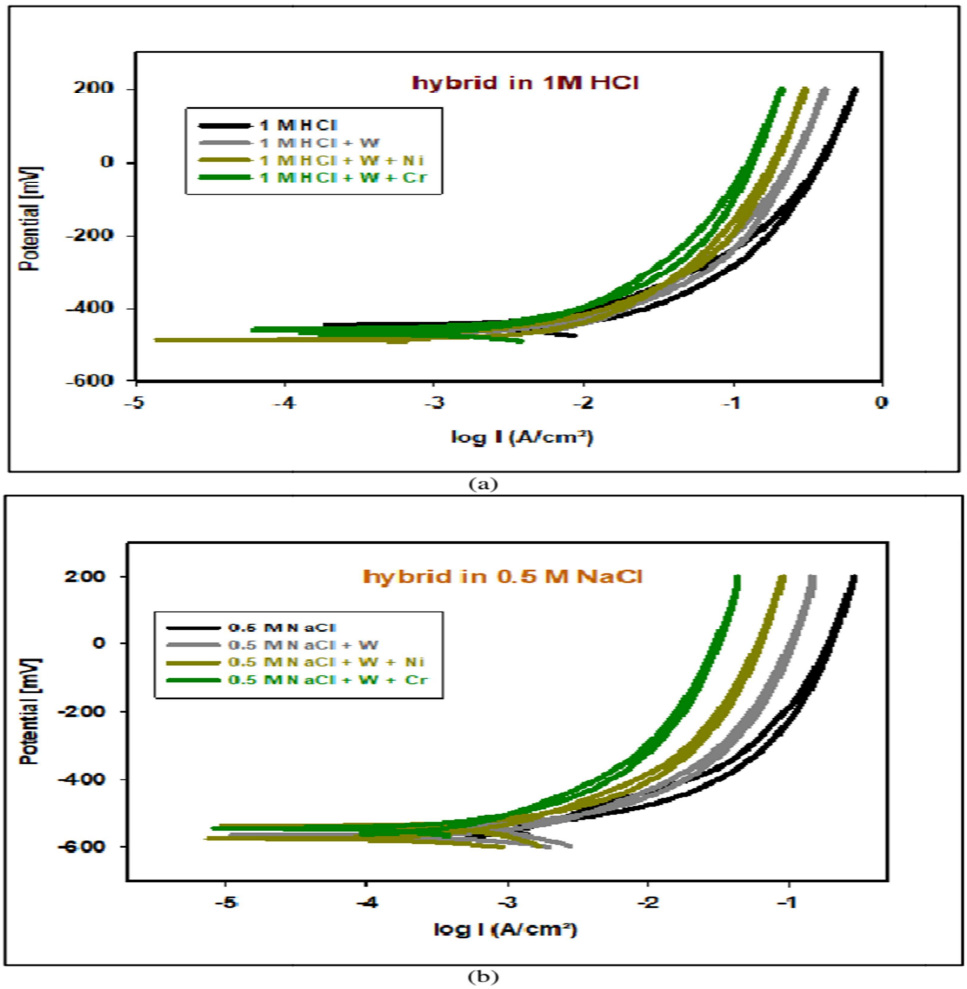

Figure 5: The CYV curves for Cu-10Ni alloy in hybrid Cr3+/ or Ni2+ with tungstate after immersion 90 days in (a) 1 M HCl and (b) 0.5 M NaCl

3.5 Surface Examination

As explained in Figs 6–15, the SEM pictures, EDX analyses, and mapping investigated the surface morphologies, chemical compositions, and elemental distribution of corrosion product coatings formed on the alloy matrix after 7 days and 90 days. After 7 days of corrosion, the surface of the sample developed small pits, and the extent of the corrosion gradually expanded over time. The resultant layer may have been constituted of cuprous oxide (Cu_2O) and cupric oxide (CuO and $Cu(OH)_2$), according to the EDX [7, 33]. The Ni corrosion that takes place on the surface of the sample degrades the performance of the film in certain areas. Inner and outer layers of Cu_2O are present in the film; the outer layer is generated by the process of deposition of dissolved Cu^{2+}. A protective and more compact Cu_2O coating constitutes the innermost layer. There are flaws, twins, or Cu matrix grain boundaries underneath the corrosion product coating. Due to their composition and structure, the corrosion product coating develops more slowly in these regions than in the intergranular. Oxidation products were produced in the outermost layer and their concentration escalated as the corrosion process progressed. The strength of the corrosion product layer is inferior to that of its internal stress.

Thus, film cracks occur due to the porosity nature of the corrosion products, which makes them easily detached from the sample. Cu-10Ni alloy SEM pictures in HCl and NaCl without hybrid Cr^{3+}/Ni^{2} with tungstate or tungstate alone. Figs 6a, 8a, 11a, and 13a demonstrate that the Cu alloy surface is highly corroded and that various corrosion products have formed on its surface. The whole surface is coated with a black corrosion result that resembles scales. In contrast, in the presence of hybrid Cr^{3+}/ or Ni^{2+} with tungstate or tungstate alone, as seen in Figs 6, 8, 11, and 13 (b, c, and d). The surface is textured with little divots. The observed morphologies indicate the absence of corrosion products. As a result, tungstate alone or hybrid Cr^{3+}/Ni^{2+} with tungstate may be used as a salt solution inhibitor to decrease the abrasiveness of Cl^- ions and improve the electrode's surface condition. Cu-10Ni alloys immersed in HCl and NaCl exhibit corrosion product deposits on their surfaces, including both a level zone and a sizable hole. This indicates that exposure to HCl and NaCl causes pitting corrosion in the Cu-10 Ni alloy. It is critical to assess the elemental composition of the Cu-10Ni alloy's surface. The percentage was ascertained using EDX analysis of the constituent composition of Cu-10Ni alloy. The EDX spectra of Cu-10Ni alloys in HCl and NaCl, with or without the hybrid Cr^{3+}/ or Ni^{2+} with tungstate, are shown in Figs 7, 9, 12, and 14 after 7 days and 90 days.

The SEM images of the Cu-10Ni alloys in 1M HCl and 0.5M NaCl after 90 days with different additions are presented in Figs. 8 and 13, respectively. While the mapping of the elemental distribution of the Cu-10Ni alloys in 1M HCl and 0.5M NaCl after 90 days with different additions are given in Fig. 10 and 15, respectively. Mapping indicates a good distribution of inhibitors in the two cases. The EDX analyses of them after 7 days and 90 days are shown in Tables 7 and 8. A rise in the duration of immersion led to a reduction in both the corrosion rate and oxygen content, except for a drop in tungstate when Cr^{3+} was introduced. It might be the result of the development of a protective coating of Cr_2O_3.

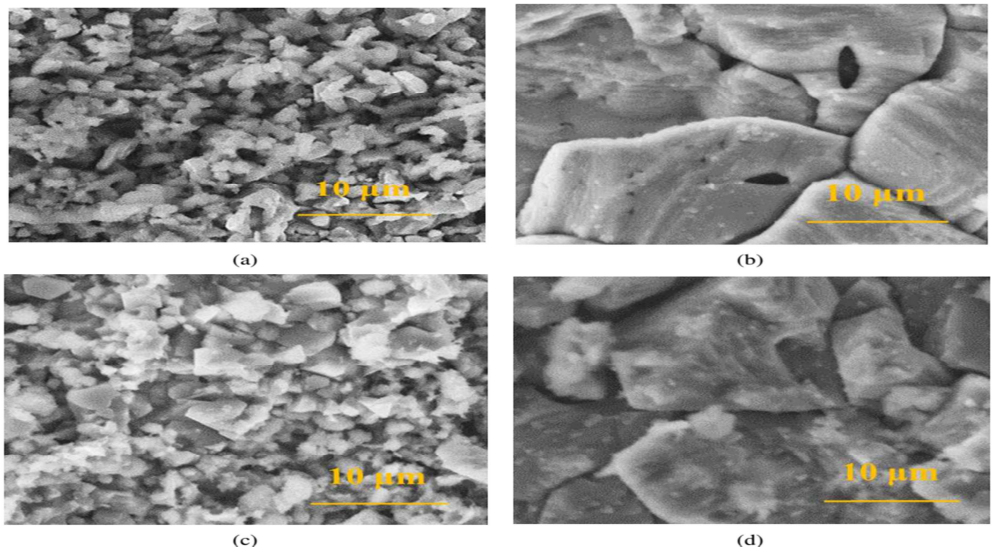

Figure 6: The SEM morphologies for the Cu-10Ni alloy after 7 days immersed in 1 M HCl with the addition of (a) zero, (b) tungstate, (C) tungstate and Cr^{3+} ions, and (d) tungstate and Ni^{2+} ions

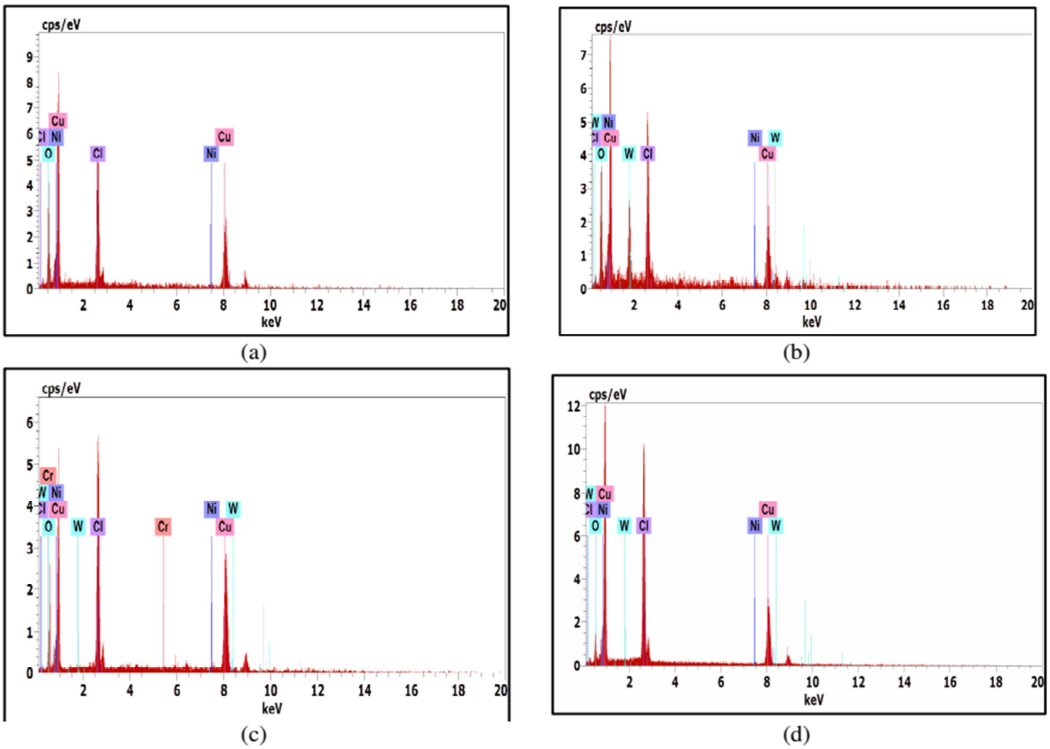

Figure 7: The EDX analyses for the Cu-10Ni alloy after 7 days immersed in 1 M HCl with the addition of (a) zero, (b) tungstate, (C) tungstate and Cr^{3+} ions, and (d) tungstate and Ni2+ ions

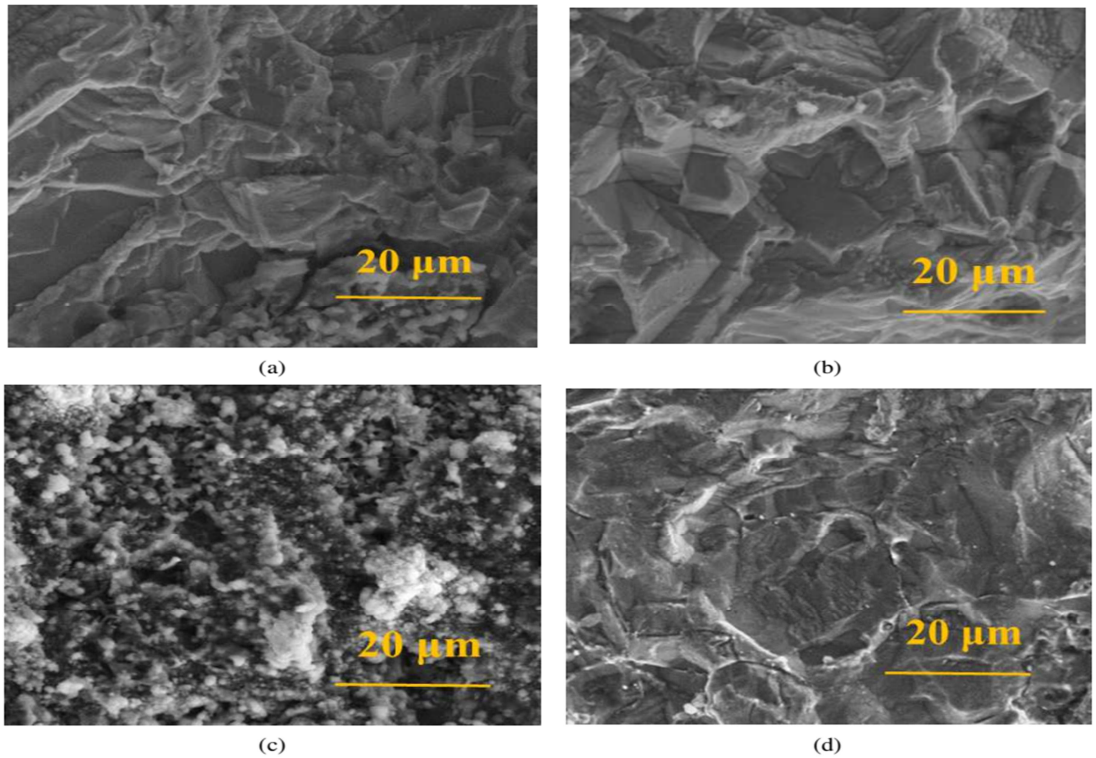

Figure 8: The SEM morphologies for the Cu-10Ni alloy after 90 days immersed in 1 M HCl with the addition of (a) zero, (b) tungstate, (C) tungstate and Cr^{3+} ions, and (d) tungstate and Ni^{2+} ions

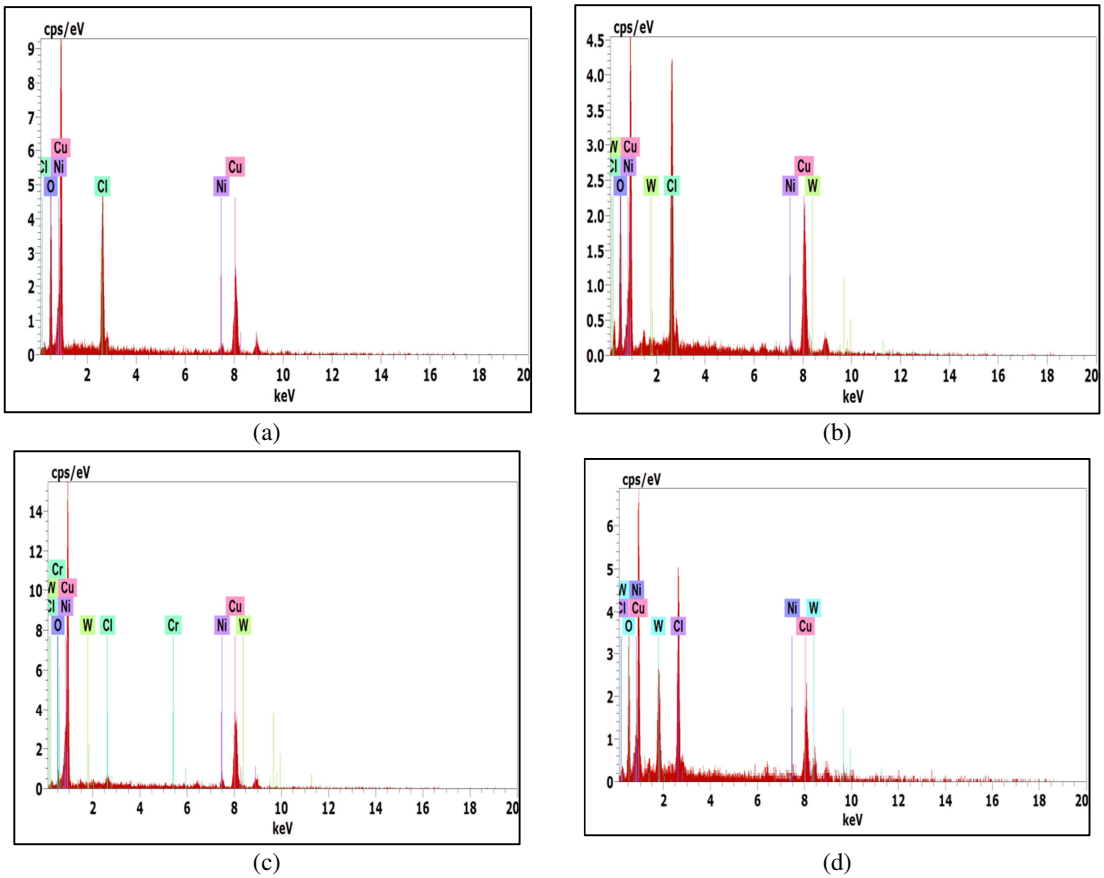

Figure 9: The EDX analyses for the Cu-10Ni alloy after 90 days immersed in 1 M HCl with the addition of (a) zero, (b) tungstate, (C) tungstate and Cr3+ ions, and (d) tungstate and Ni2+ ions

Table 7. The EDX results for different conditions after 7 and 90 days in 1M HCl media

Inhibitors	Days	Elements, wt.%					
		Cl	O	Ni	W	Cr	Cu
Cu-Ni alloy	7	23.6	21.8	0.6	--	--	Bal.
	90	15.7	33.2	3.0	--	--	Bal.
Cu-Ni alloy +(W)	7	31.0	11.6	1.0	0.1	--	Bal.
	90	18.0	24.6	2.7	0.2	--	Bal.
Cu-Ni alloy +(W+Cr)	7	35.2	11.4	0.8	0.2	0.2	Bal.
	90	2.0	4.2	8.0	1.4	0.3	Bal.
Cu-Ni alloy +(W+Ni)	7	15.6	28.6	1.1	19.2	--	Bal.
	90	0.3	3.5	10.0	1.5	--	Bal.

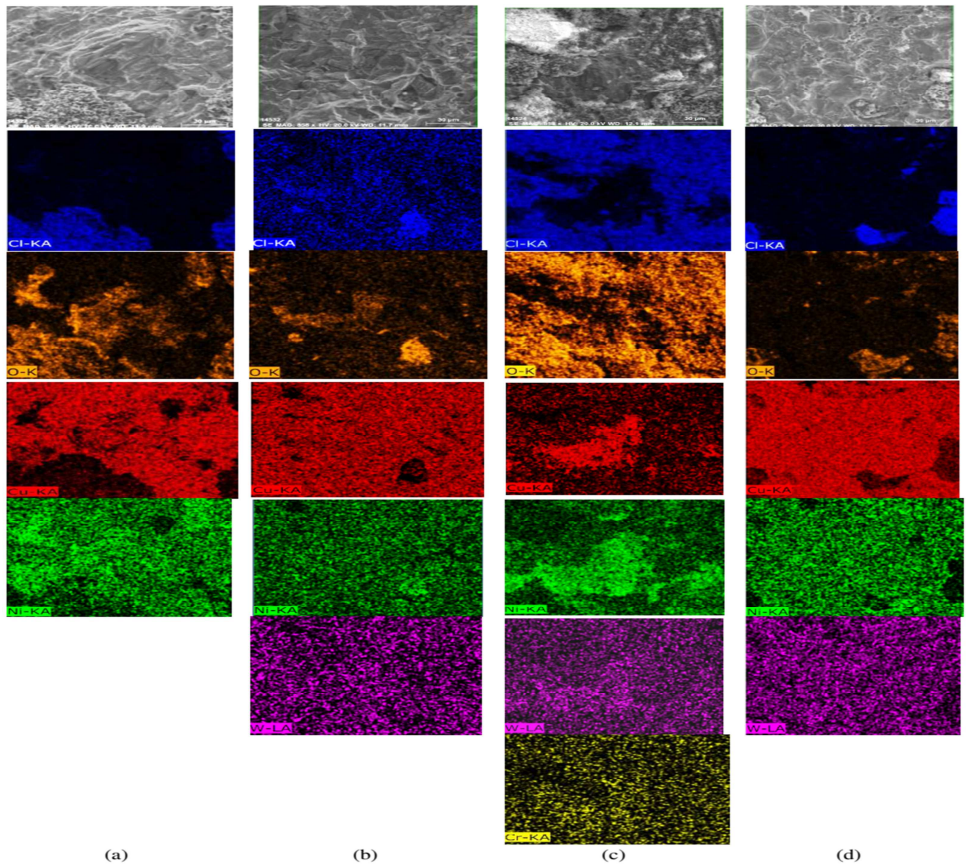

Figure 10: Mapping of Cu-10 Ni in 1M HCl for 90 days (a) Cu-10Ni, (b) Cu-10Ni +W, (c) Cu-10Ni+(W+Cr), and (d) Cu-10Ni +(W+Ni)

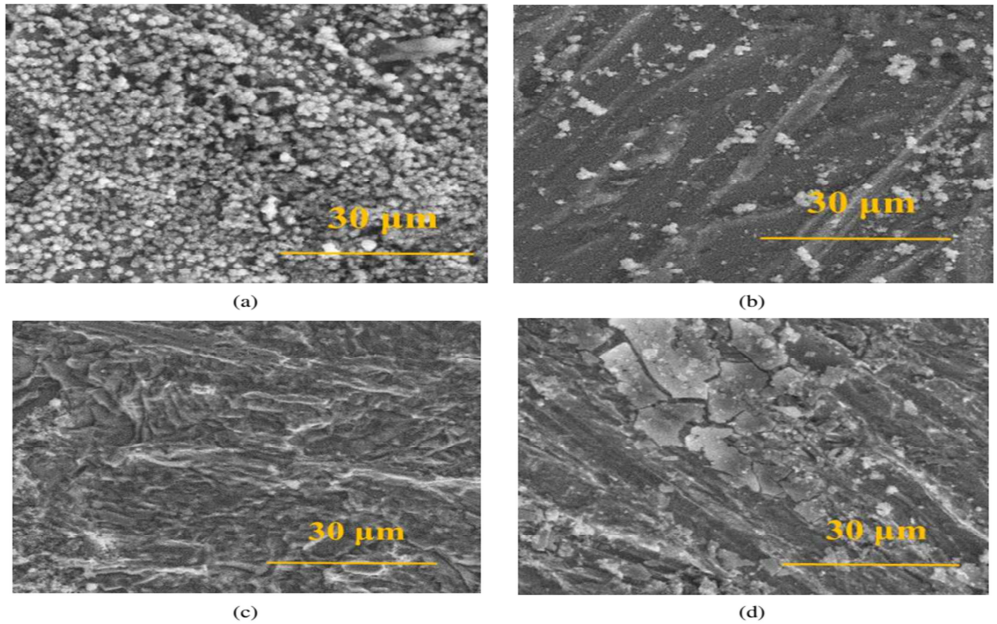

Figure 11: The SEM morphologies for the Cu-10Ni alloy after 7 days immersed in 0.5 M NaCl with the addition of (a) zero, (b) tungstate, (C) tungstate and Cr3+ ions, and (d) tungstate and Ni2+ ions

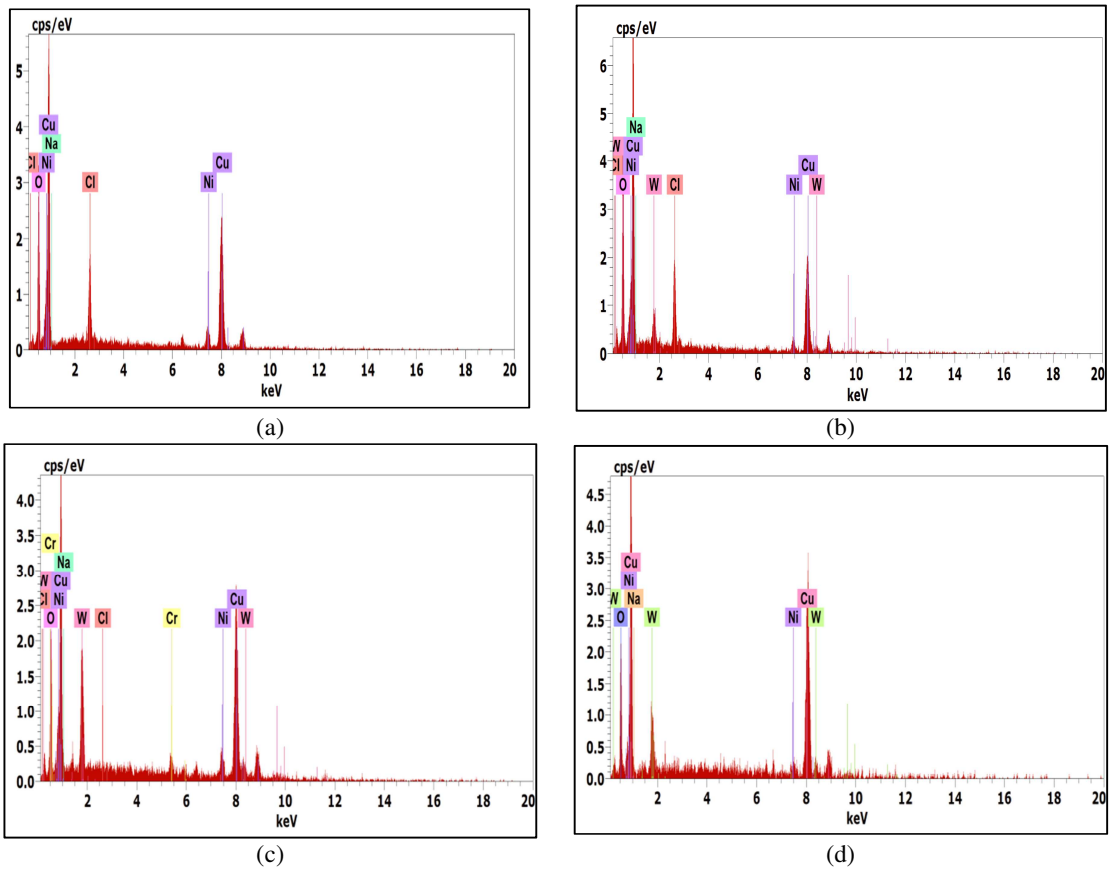

Figure 12: The EDX analyses for the Cu-10Ni alloy after 7 days immersed in 0.5 M NaCl with the addition of (a) zero, (b) tungstate, (C) tungstate and Cr^{3+} ions, and (d) tungstate and Ni^{2+} ions

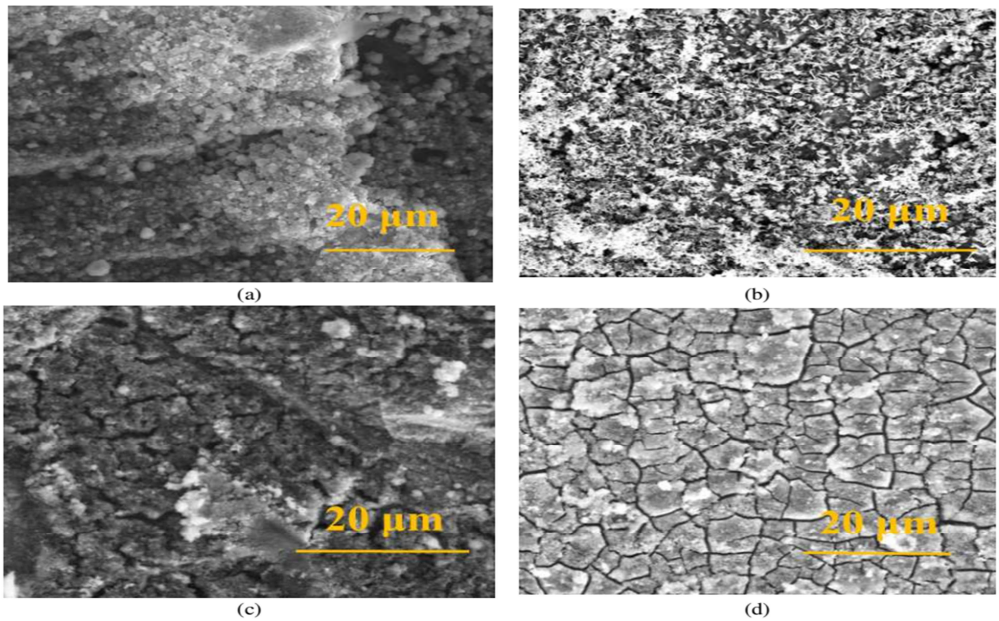

Figure 13: The SEM morphologies for the Cu-10Ni alloy after 90 days immersed in 0.5 M NaCl with the addition of (a) zero, (b) tungstate, (C) tungstate and Cr^{3+} ions, and (d) tungstate and Ni^{2+} ions

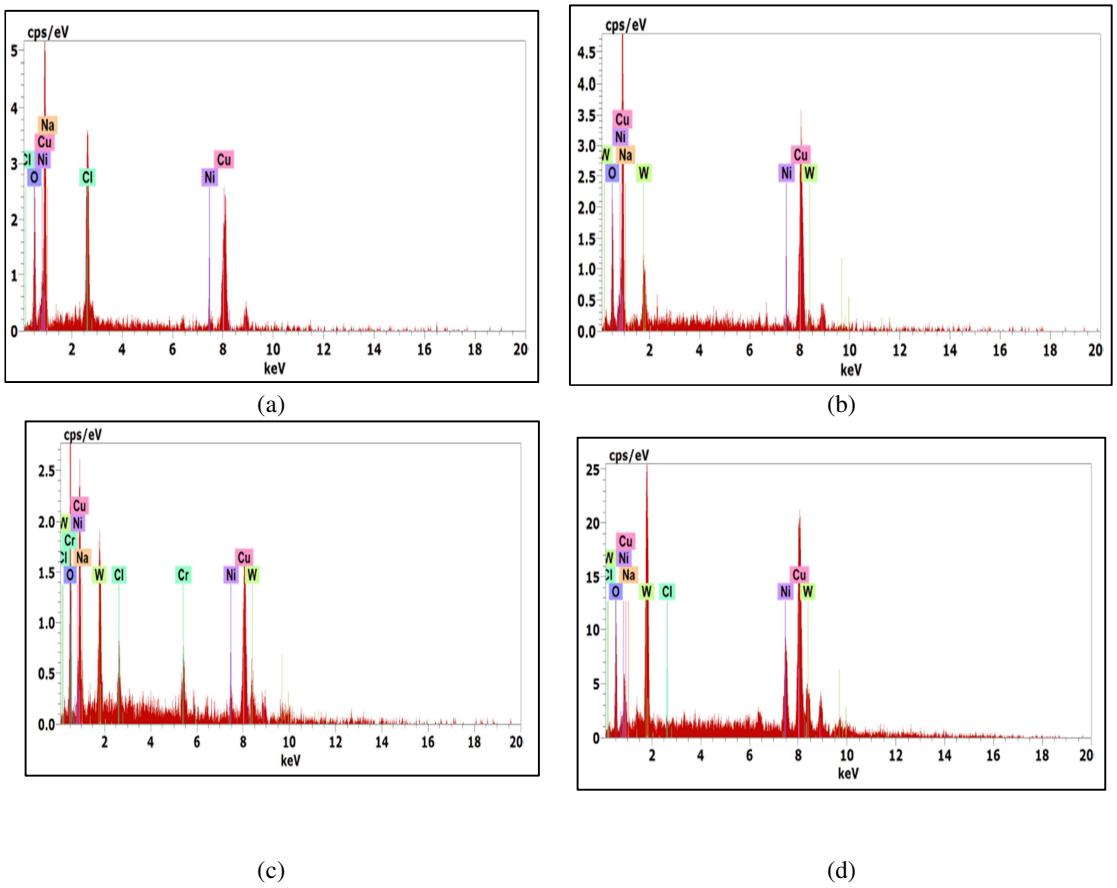

Figure 14: The EDX analyses for the Cu-10Ni alloy after 90 days immersed in 0.5 M NaCl with the addition of (a) zero, (b) tungstate, (C) tungstate and Cr^{3+} ions, and (d) tungstate and Ni^{2+} ions

Table 8. The EDX results for different conditions after 7 and 90 days in 0.5M NaCl media

Inhibitors	Days	Elements, wt.%						
		Na	Cl	O	Ni	W	Cr	Cu
Cu-Ni alloy	7	--	7.2	25.7	6.7	--	--	Bal.
	90	0.7	11.5	22.9	3.3	--	--	Bal.
Cu-Ni alloy +(W)	7	0.6	8.0	32.2	3.6	4.5	--	Bal.
	90	--	0.2	15.1	4.9	9.0	--	Bal.
Cu-Ni alloy +(W+Cr)	7	0.4	0.2	16.4	6.6	10.4	2.1	Bal.
	90	4.2	2.7	26.4	3.3	18.0	5.2	Bal.
Cu-Ni alloy +(W+Ni)	7	--	--	13.1	9.56	8.1	--	Bal.
	90	0.1	0.1	10.2	12.4	26.5	--	Bal.

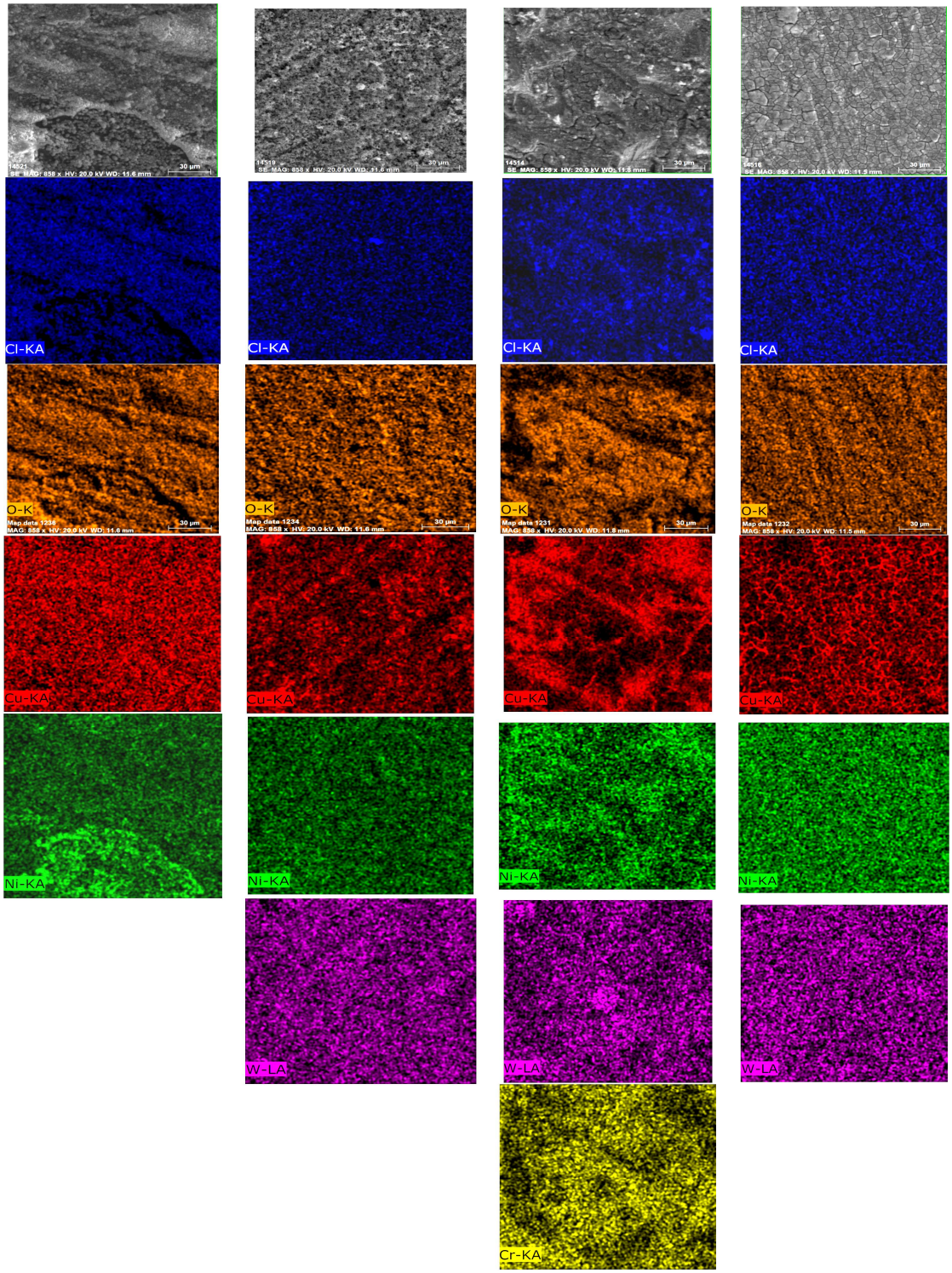

(a) (b) (c) (d)

Figure 15: Mapping of Cu-10 Ni in 0.5M NaCl For 90 days (a) Cu-10Ni, (b) Cu-10Ni +W, (c) Cu-10Ni+(W+Cr), and (d) Cu-10Ni +(W+Ni)

Corrosion Mechanism

Redox corrosion describes the behaviour of Cu-Ni alloys in a neutral chloride solution [34]. At the same concentration, Cl^- reacts with Cu^+ more readily than OH^- in the chloride solution [35]. Consequently, the

primary agent accountable for the deterioration of Cu or Cu alloys when exposed to saltwater is Cl^-.The cathodic reaction entails the reduction of oxygen, while the anode reaction includes the dissolution of Cu [34]. The procedure for a cathodic reaction is:

$$O_2 + 2H_2O + 4e^- \leftrightarrow 4OH^- \quad (6)$$

The dissolution of Cu form to cuprous dichloride anion ($CuCl^{2-}$) is the anodic reaction, which is believed to be the primary dissolving mechanism in saltwater or NaCl [36, 37].

$$Cu + 2Cl \leftrightarrow CuCl^{2-} + e^- \quad (7)$$

A rise in the surface concentration of $CuCl^{2-}$ initiates a hydrolysis reaction (Cu_2O formation) [38, 39] as in the following reaction:

$$2CuCl_2 + 2H_2O \leftrightarrow Cu_2O + 4Cl^- + 2H^+ \quad (8)$$

Based on the Pourbaix diagram of Cu [40], when exposed to saltwater at a temperature of 25 °C and under experimental circumstances, Cu_2O retains the capacity to undergo oxidation to CuO or $Cu_2(OH)_3Cl$ at the corrosion product surface via Eqs (9) and (10) [6]:

$$Cu_2O + H_2O \leftrightarrow 2CuO + 2H+ + 2e^- \quad (9)$$

$$Cu_2O+Cl- + 2H_2O \leftrightarrow Cu_2(OH)_3Cl + H+ + 2e^- \quad (10)$$

The Ni^{2+} contribution to improving sample surface film protectivity. The addition of CuO, NiO, $Cu(OH)_2$, and $Ni(OH)_2$ to the produced surface film may have improved the Ni^{2+}, making the film more protective [12]. Local acidification inside the pores of the corrosion products is readily possible in a highly concentrated chloride solution [41]. Therefore, Eq. (9) predominates throughout the re-oxidation process of Cu_2O. Cu_2O is deficient in p-type semiconductor elements. A drop in Cu_2O content and a rise in CuO and $Cu(OH)_2$ content are seen on the surface of the sample. This results in a reduction in electron conductivity and an improvement in CRST. Additional Cu oxidation may be expressed as:

$$Cu_2O + O_2 + H_2O \leftrightarrow 2CuO + H_2O_2 \quad (11)$$

$$Cu_2O + 3H_2O \leftrightarrow 2Cu(OH)_2 + 2H^+ + 2e^- \quad (12)$$

The addition of tungsten led to enhanced CRST of the alloys due to the passive layer WO_3 formation increasing with the increase in the content of tungsten [42]. The anodic process is the dissolution of tungsten as in Eq. 13 [43]:

$$W + 4H_2O \rightarrow \ WO_4^{2-} \ + 8H^+ + 6e^- \quad (13)$$

At elevated temperatures, the mechanical, oxidation, and CRST properties of other metals are enhanced by the addition of Ni [44]. Eqs. 14 and 15 [45] demonstrate that Ni may include NiO and $Ni(OH)_2$.

$$Ni + H_2O \rightarrow Ni(OH)_2 + 2H^+ + 2e^- \quad (14)$$

$$Ni(OH)_2 \rightarrow NiO + 2H^+ + 2e^- \quad (15)$$

As seen in Fig. 7, a schematic depicting the chemical constitute of the Cu-Ni alloy's surface layers at various depths is the consequence of each of these findings. The oxygen ions undergo a fast reaction with the metal at the interface of the two substances, resulting in the formation of oxides. This process produces oxygen that is chemically active and further enhances the chemical interaction between the oxygen ions and the metal ions. With the extension of the treatment time, the oxide film undergoes external expansion, leading to the development of a significant layer on the surface of the alloy [46, 47]. Therefore, the CRST of Cu-Ni alloy immersed in a 3.5% NaCl solution may experience an elevation. This can be attributed to the generation of cation vacancies at the Cu-Ni film interface, which is caused by the Ni ions' diffusion rate from the Ni-film interface to the film-solution interface.

The Cr concentration enhances the passivation capability of alloys in chloride-containing aqueous solutions, hence enhancing the passive coating's durability and pitting CRST. This is due to the formation of Cr_2O_3. In contrast, excessive Cr induces severe pitting corrosion owing to Cr segregation as in Eq. 16 [13, 47].

$$2Cr + 3H_2O \rightarrow Cr_2O_3 + 6H^+ + 6e^- \quad (16)$$

Cr_2O_3 decreases the substrate's active surface area and encourages Cu_2O to grow as a cathode. The entire Cu_2O layer that accumulates during outward re-precipitation plays a major role in controlling the alloy's corrosion process as immersion time increases. Because the radii of Cr^{3+} and Cu^+ are comparable, it has previously been reported that Cr might be integrated into the Cu_2O lattice [13]. According to the findings of POT curves, the addition of Cr may help increase the corrosion film's resistance even further. The corrosion behaviour of the Cu-10Ni alloy thus indicates that the addition of Cr^{3+} raises the protective ability of the corrosion film [13].

Conclusion

The Cu-10Ni alloy corrosion characteristics in hybrid Cr^{3+} or Ni^{2+} with tungstate in 1M and 0.5M NaCl for 7 and 90 days can be summarized as the following:

1. A hybrid Cr^{3+}/ or Ni^{2+} formulation with tungstate or tungstate alone can serve as a potent inhibitor to prevent the occurrence of corrosion of Cu-10Ni alloy in 1 M HCl and 0.5 M NaCl.
2. The OCP revealed that after seven days of exposure, the E_{corr} switched in a positive direction due to the protective oxide film inhibiting effect on the corrosion of the Cu-10Ni surface, which occurred because of the

reduction in reaction rate and the Cl^- attack on the surface. The tungstate-hybrid Cr^{3+} exhibits a remarkable corrosion efficiency index percent (IE%) of around 82% in 1M HCl and 68% in 0.5M NaCl.

3. POT and CYV plots show that the additions of Cr^{3+} with tungstate to Cu-10Ni alloys have the best CRST in two acidic media (0.5 NaCl, 1 HCl). The CR values of Cu-10Ni alloy are 20.03 and 3.53 mm/y in 1 M HCl and 0.5 M NaCl, respectively.
4. The corrosion byproduct that formed on the surface of the Cu-10Ni alloy consisted mostly of CuO, Cu_2O, and $Cu(OH)_2$. An extension in the duration of exposure led to the deposition of CuCl, $CuCl_2$, and $Cu_2(OH)_3Cl$ on the alloy's surface, therefore affording a modest level of resistance against corrosion. Thus, these enhance the corrosion resistance of Cu-10Ni alloy in industrial applications.

Although the Cu-Ni alloys have a variety of applications in marine engineering we will investigate in the future work the corrosion evolution in various corrosive media using environmentally friendly waste products.

Conflict of interest

The authors declare that they have no conflicts of interest.

References

[1]. A. M. El-Shamy, Y. Reda, K. M. Zohdy, A.K. Eessaa, Effect of Plating Materials on the Corrosion Properties of Steel Alloy 4130, Egypt. J. Chem. Vol. 63, No. 2. pp.579-597 (2020)

[2]. M.M. Megahed, M.Y. Sedeka, A.M. El-Shamy, Selective Formula as a Corrosion Inhibitor to Protect the Surfaces of Antiquities Made of Leather-Composite Brass Alloy, Egypt. J. Chem. Vol. 63, No. 12 pp. 5269 - 5287 (2020)

[3]. A. M. El-Shamy, A Review On: Biocidal Activity of Some Chemical Structures and Their Role in Mitigation of Microbial Corrosion, Egypt. J. Chem. Vol. 63, No. 12 pp. 5251 - 5267 (2020)

[4]. C. Xia, C. Ni, Y. Pang, Y. Jia, S. Deng, W. Zheng, Study of Coarse Particle Types, Structure and Crystallographic Orientation Relationships with Matrix in Cu-Cr-Zr-Ni-Si Alloy, Crystals 2023, 13, 518

[5]. S. Yazdani, V. Vitry, Using Molecular Dynamic Simulation to Understand the Deformation Mechanism in Cu, Ni, and Equimolar Cu-Ni Polycrystalline Alloys, Alloys 2023, 2, 77–88.

[6]. G. Shao, Y. Gao, J. Wu, P. Liu, K. Zhang, W. Li, F. Ma, H. Zhou, X. Chen, Effect of Fe/Mn content on mechanical and corrosion properties of 90/10 copper–nickel alloy, Materials and Corrosion. 2022; 73:1085–1098.

[7]. C.C. Nwaeju, A.O. Eboh, F.O. Edoziuno, Grain size evolution, mechanical and corrosion behaviour of precipitate strenthened Cu-Ni alloy, Acta Metallurgica Slovaca, 2022, 28(4), 188-196

[8]. E.M. Sherif, A.A. Almajid, A.K. Bairamo, E. Al-Zahrani, A comparative Study on the Corrosion of Monel-400 in Aerated and Deaerated Arabian Gulf Water and 3.5% Sodium Chloride Solutions, Int. J. Electrochem. Sci., 7, 2796– 2810, (2012).

[9]. G. A. Gaber, M.A. Maamoun, W.A. Ghanem, Evaluation of the Inhibition Efficiency of a Green Inhibitor on Corrosion of Cu-Ni Alloys in the Marine Application, Key Eng. Mater. 786 (2018) 174-194

[10]. S. Hu, L. Liu, Y. Cui, Y. Li, F. Wang, Influence of hydrostatic pressure on the corrosion behavior of 90/10 copper-nickel alloy tube under alternating dry and wet condition. Corros. Sci. 2019, 146, 202–212

[11]. L. Wu, A. Ma, L. Zhang, G. Li, L. Hu, Z. Wang, Y. Zheng, Erosion–Corrosion Behavior of 90/10 and 70/30 Copper–Nickel Tubes in 1 wt% NaCl Solution, Metals 2023, 13, 401.

[12]. M. F. Shehata, S.E. El-Shafey, N.S. Ammar, A.M. El-Shamy, Reduction of Cu+2 and Ni^{+2} Ions from Wastewater Using Mesoporous Adsorbent: Effect of Treated Wastewater on Corrosion Behavior of Steel Pipelines, Egypt. J. Chem. Vol. 62, No. 9. pp. 1587 - 1602 (2019)

[13]. S. Li, M. Fang, Z. Xiao, X. Meng, Q. Lei, Y. Jia, Effect of Cr addition on corrosion behavior of cupronickel alloy in 3.5 wt.% NaCl solution, Journal of materials research and technology, 2023; 22: 2222-2238

[14]. O.O. Ekerenam, A.-L. Ma, Y.-G. Zheng, S.-Y. He, P.C. Okafor, Evolution of the Corrosion Product Film and Its Effect on the Erosion–Corrosion Behavior of Two Commercial 90Cu–10Ni Tubes in Seawater, Acta Metallurgica Sinica (English Letters) (2018) 31:1148–1170

[15]. Y. Zhang, C. Song, Y. Cao, H. Wang, Z. Wang, B. Yang, Microstructure and Corrosion Behavior of as-cast 90Cu-10Ni Alloys with Different Yttrium Content, Int. J. Electrochem. Sci., 15 (2020) 4161 – 4178

[16]. A.M. Nattah, A.M. Salim, N.M. Dawood, Influence of nano chromium addition on the corrosion and erosion–corrosion behavior of cupronickel 70/30 alloy in seawater, Open Engineering 2023; 13: 20220491

[17]. G.A. Gaber,H.A. Aly, L.Z. Mohamed, Effect of Sodium Tungstate on the Corrosion Behavior of FeBase Alloy in H2SO4 Solution, Int. J. Electrochem. Sci., 15 (2020) 8229 – 8240

[18]. A.M. Al-Sabagh, N.G. Kandile, N.M. Nasser, M.R. Mishrif, A.E. El-Tabey, Novel surfactants incorporated with 1,3,5-triethanolhexahydro-1,3,5-triazine moiety as corrosion inhibitors for carbon steel in hydrochloric acid: Electrochemical and quantum chemical investigations, Egypt. J. Pet., 22 (2013) 351-365

[19]. S. Garai, S. Garai, P. Jaisankar, J. Singh, A. Elango, A comprehensive study on crude methanolic extract of Artemisia pallens (Asteraceae) and its active component as effective corrosion inhibitors of mild steel in acid solution, Corros. Sci., 60 (2012) 193-204

[20]. A. M. El-Shamy, M. Abdelbar, Ionic Liquid as Water Soluble and Potential Inhibitor for Corrosion and Microbial Corrosion for Iron Artifacts, Egypt. J. Chem. Vol. 64, No. 4 pp. 1867 - 1876 (2021)
[21]. M.M. Megahed, M.M. Abdelbar, E.M. Abouelez, A.M. El-Shamy, Polyamide Coating as a Potential Protective Layer Against Corrosion of Iron Artifacts, Egypt. J. Chem. Vol. 64, No 10 pp. 5693 – 5702 (2021)
[22]. S.M. Mouneir, A.M. El-Hagrassi, A.M. El-Shamy, A Review on the Chemical Compositions of Natural Products and Their Role in Setting Current Trends and Future Goals, Egypt. J. Chem. Vol. 65 No. 5 pp. 491 – 506 (2022)
[23]. S. A. Kanimozhi, S. Rajendran, Realization of synergism in sodium tungstate-Zn2+-N-(Phosphenomethyl) iminodiacetic acid system in well water, Open Corros. J. 2 (2009) 166-174
[24]. G. Mu, X. Li, Q. Qu, J. Zhou, Molybdate and tungstate as corrosion inhibitors for cold rolling steel in hydrochloric acid solution, Corrosion Science 48 (2006) 445–459.
[25]. Q.J. Xu, G.D. Zhou, H.F. Wang, W.B. Cai, Electrochemical studies of polyaspartic acid and sodium tungstate as corrosion inhibitors for brass and Cu30Ni alloy in simulated cooled water solutions, Anti-Corrosion Methods and Materials, 53 (2006) 207-211.
[26]. R. Khandelwal, SK. Arora, SP. Mathur, Study of Plant Cordia Dichotoma as Green Corrosion Inhibitor for Mild Steel in Different Acid Media. E-J Chem, 3 (2011) 1200-1205
[27]. A. Abdelfatah, L.Z. Mohamed, G.A. Gaber, Corrosion Inhibition of Hybrid Ti/Ce Salt for Zinc in HCl Solution, Egypt. J. Chem. Vol. 66, No. SI 13, 1069-1079 (2023)
[28]. G.A. Gaber, L.Z. Mohamed, A. Abdelfatah, Study the corrosion issues on galvanized steel induced in water tanks, Chemical Papers (2023) 77:7539–7549.
[29]. S. Rajendran, S.P. Sridevi, N. Anthony, A.J. Amalraj, M. Sundaravadivelu, Corrosion behaviour of carbon steel in polyvinyl alcohol, Anti-Corrosion Methods and Materials, 52 (2005) 102-107
[30]. X. Zhang, Y.Q. Chen, S. Zhao, F. Han, X. Xiang, Y.C. Zhao, N. Huang, G.J. Wan, Surface electronic properties, super-hydrophilicity and bending strength. Mater. Des. 89 (2016) 476–484
[31]. A. Ma, S. Jiang, Y. Zheng, W. Ke, Corrosion product film formed on the 90/10 copper–nickel tube in natural seawater: Composition/structure and formation mechanism, Corrosion Science, 91, 245–261, (2015).
[32]. N.K. Awad, E.A. Ashour, N.K. Allam. Unravelling the composition of the surface layers formed on Cu, Cu-Ni, Cu-Zn and Cu-Ni-Zn in clean and polluted environments, Appl. Surf. Sci. 346 (2015) 158–164
[33]. T. Jin, W. Zhang, N. Li, X. Liu, L. Han, W. Dai, Surface Characterization and Corrosion Behavior of 90/10 Copper-Nickel Alloy in Marine Environment, Materials, 12 (2019) 1869.
[34]. T. Xia, L. Zeng, X. Zhang, J. Liu, W. Zhang, T. Liang, B. Yang, Enhanced corrosion resistance of a Cu-10Ni alloy in a 3.5 wt% NaCl solution by means of ultrasonic surface rolling treatment Surface & Coatings Technology, 363, 390–399, (2019).
[35]. B. Sun, T. Ye, Q. Feng, J. Yao, M. Wei, Accelerated Degradation Test and Predictive Failure Analysis of B10 Copper-Nickel Alloy under Marine Environmental Conditions, Materials, 8, 6029–6042, (2015).
[36]. S. Neodo, D. Carugo, J.A. Wharton, K.R. Stokes, Electrochemical behavior of nickel–aluminium bronze in chloride media: Influence of pH and benzotriazole, Journal of Electroanalytical Chemistry, 695, 38–46, (2013).
[37]. H.N. Krogstad, R. Johnsen, Corrosion properties of nickel-aluminium bronze in natural seawater—Effect of galvanic coupling to UNS S31603, Corrosion Science, 121, 43–56, (2017).
[38]. W.A. Badawy, M. El-Rabiee, N.H. Helal, H. Nady, The role of Ni in the surface stability of Cu– Al–Ni ternary alloys in sulfate–chloride solutions, Electrochimica Acta, 71, 50–57, (2012).
[39]. A.A. El Warraky, A.E. El Meleigy, Sh.E. Abd El Hamid, The Electrochemical Behavior of 70-30 Cu-Ni Alloy in LiBr Solutions, Egypt. J. Chem. 59 (5), 833- 850, (2016).
[40]. G.A. Gaber, W.A. Hussein, A.S.I. Ahmed, Comparative Study of Electrochemical Corrosion of Novel Designs of 90/10 and 70/30 Copper-Nickel Alloys in Brine Solutions, Egypt. J. Chem. Vol. 63,No. 4, pp. 1527-1540 (2020)
[41]. S.A. Campbell, G.J.W. Radford, C.D.S. Tuck, B.D. Barker, Corrosion and Galvanic Compatibility Studies of a High-Strength Copper- Nickel Alloy, Corrosion, 58, 57–71, (2002).
[42]. D. Kumar, O. Maulik, V.K. Sharma, Y.V.S.S. Prasad, V. Kumar, Understanding the Effect of Tungsten on Corrosion Behavior of AlCuCrFeMnWx High-Entropy Alloys in 3.5 wt.% NaCl Solution, Journal of Materials Engineering and Performance, 2018
[43]. A.S. Racz, Z. Kerner, M. Menyhard, Corrosion resistance of tungsten carbide-rich coating layers produced by noble gas ion mixing, Applied Surface Science, 605, 15, 2022, 154662.
[44]. L.Z. Mohamed, K.A. Abdelghafar, H.A. Aly, G.A. Gaber, Comparative studies of Cr/Ti additions for Cu40Mn25Al20Fe5Ni5 HEA on microstructure and corrosion behaviour in HNO3 solution, International Journal of Metalcasting, 17(3), 2023, 1791-1805
[45]. L.Z. Mohamed, M.A.H. Gepreel, A. Abdelfatah, Corrosion behavior of Al12Cr12Fe35Mn21Ni20 high entropy alloy in different acidic media, Chemical Papers (2021) 75:6265–6274
[46]. S.P. Chenakin, B.N. Mordyuk, N.I. Khripta, Surface characterization of a ZrTiNb alloy: Effect of ultrasonic impact treatment, Applied Surface Science, 470, 44–55, (2019).
[47]. M.A. Vasylyev, S.P. Chenakin, L.F. Yatsenko, Ultrasonic impact treatment induced oxidation of Ti6Al4V alloy, Acta Materialia, 103, 761–774, (2016).